Pharmaceutical Science Advances 3 (2025) 100079

Contents lists available at ScienceDirect

Pharmaceutical Science Advances

journal homepage: www.journals.elsevier.com/pharmaceutical-science-advances

Artificial neural network guided optimization of tenofovir and Cyanovirin-N multipurpose preventive hydrogel formulation developed using the Box Behnken design model

Karamot O. Oyediran [a,*], Ibilola M. Cardoso-Daodu [a], Peace Ofonabasi Bassey [a], Deborah A. Ogundemuren [a], Ridwan Muhammed [a,f], Olusola E. Ojo [b], Andrew N. Amenaghawon [c], Chukwuemeka P. Azubuike [a], Rachna Agarwal [d,e], Kondoru Haritha [d,e], Margaret O. Ilomunaya [a,f,**]

[a] Department of Pharmaceutics and Pharmaceutical Technology, Faculty of Pharmacy, University of Lagos, PMB 12003, Lagos, Nigeria
[b] Department of Metallurgical and Materials Engineering, Faculty of Engineering, University of Lagos, Lagos, Nigeria
[c] Department of Chemical Engineering, Faculty of Engineering, University of Benin, Benin City, Nigeria
[d] Bhabha Atomic Research Centre Mumbai, 400085, India
[e] Homi Bhabha National Institute, Training School Complex, Anushaktinagar, Mumbai, 400 094, India
[f] MEDAFRICA GMP Laboratory, Faculty of Pharmacy University of Lagos, PMB 12003, Lagos, Nigeria

ARTICLE INFO

Keywords:
Box Behnken design
Artificial neural network
Hydrogels
Cyanovirin-N
Tenofovir
Flux

ABSTRACT

Tenofovir (TNF) is an antiretroviral drug that has being used as a topical microbicide to prevent human immunodeficiency virus transmission (HIV). Cyanovirin-N (CV-N) is a lectin protein that can bind to the HIV envelope glycoprotein and inhibit viral entry. The combination of TNF and CV-N may have synergistic effects and enhance the efficacy of microbicide. The aim of this study was to develop and optimize composite hydrogel formulations containing 1%TNF and 0.0005% CV-N using Box Behnken Design. A three-factor, three-level Box-Behnken design was employed to investigate the effects of the concentrations of PEG_{2000}, sodium carboxyl methylcellulose (NaCMC), and calcium chloride on the release of Tenofovir, flux, and mucoadhesion. The mucoadhesion was evaluated by measuring the percent mucin adsorption while flux and release kinetics were evaluated using the Franz cell diffusion method. The optimal hydrogel formulation was found to contain 4% NaCMC, 2% PEG2000 and 1% $CaCl_2$. The hydrogel had a pH of 4.5 ± 0.017, a viscosity of 275600 ± 0.65 cP, flux 9806 μg/cm^2/h for TNF with a drug release of 119, 205.6 μg/cm^2. The TNF gel exhibited a pseudoplastic rheological behavior with 96.3% muco-adhesion. The study successfully developed an optimized TNF/CV-N mucoadhesive hydrogel, highlighting its potential as an on-demand multipurpose prevention technology (MPT) for HIV. The formulation was optimized to ensure good drug release, flux and mucoadhesion. The optimized hydrogel offers a convenient, effective method for preventing sexually transmitted infections (STIs), addressing critical challenges in drug delivery and user adherence while advancing public health strategies for STIs.

1. Introduction

The soaring rates of human immunodeficiency virus (HIV) and sexually transmitted infections (STIs) highlight an urgent need for more effective prevention strategies. Challenges encountered with current HIV and STI-prophylactic measures have significantly impacted the effectiveness of these measures especially in resource limited countries. From the advent of condoms to the use of microbicides, the search for newer technologies that are more effective, less toxic, discreet, and time

* Corresponding author.
** Corresponding author. Department of Pharmaceutics and Pharmaceutical Technology, Faculty of Pharmacy, University of Lagos, PMB 12003, Lagos, Nigeria.
E-mail addresses: karamahtobi@yahoo.com (K.O. Oyediran), icardoso@unilag.edu.ng (I.M. Cardoso-Daodu), ofonabasi63@gmail.com (P.O. Bassey), ogundemurendeborah@gmail.com (D.A. Ogundemuren), ridwanmuhd411@gmail.com (R. Muhammed), isolyet@yahoo.com (O.E. Ojo), andrew.amenaghawon@uniben.edu (A.N. Amenaghawon), cazubuike@unilag.edu.ng (C.P. Azubuike), rachna@barc.gov.in (R. Agarwal), harithak@barc.gov.in (K. Haritha), milomuanya@unilag.edu.ng (M.O. Ilomunaya).

https://doi.org/10.1016/j.pscia.2025.100079
Received 4 February 2025; Received in revised form 13 June 2025; Accepted 17 June 2025

List of abbreivations

MPTs	Multipurpose Preventive Technologies
PEG	Polyethylene Glycol
CCD	Central composite design
ANN	Artificial neural network
FFNA	feed forward neural architecture
CV-N	Cyanovirin-N
MSE	Mean square error
SEP	Standard error of prediction
RMSE	Root mean square error
R	Correlation coefficient
R^2	Coefficient of determination
SEM	Scanning electron microscope
H&E	Hematoxylin and eosin

sensitive use continues [1]. Multipurpose prevention technologies (MPTs) are products designed to cater to multifarious reproductive health prophylaxis such as HIV/STI prophylaxis and contraception. However, MPTs face challenges in formulation, user acceptability, and co-delivery of multiple agents [2].

Several products are currently under development ranging from non-antiretrovirals (ARV)/non hormonal multipurpose intra-vaginal ring, griffithsin fast dissolving vaginal inserts, to antiretrovirals co-formulated with hormonal contraceptives such as cabotegravir/levonorgestrel injectable or implant, dapivirine/levonorgestrel among others [2]. Despite the success recorded in this field, research amongst the end users has indicated the need for a wider range of products, dosage forms, designs, ease of use, long duration of action, and more discreet products [3–6]. Also, challenges with delivering two or more drugs with different doses and physicochemical characteristics make development of an ideal multipurpose preventive product a challenge. The search for an effective, affordable and widely acceptable multipurpose preventive technology, that is discreet, easy to use, and safe is paramount to curtail the scourge of HIV and STIs.

Cyanovirin N (CV-N), a 101 amino acid protein derived from the Cyanobacterium *Nostoc ellipsosporum* has demonstrated potency against several enveloped viruses, including multiple strains of HIV, Simian immunodeficiency virus, Human papillomavirus, Herpes simplex, Ebola, influenza, and Hepatitis C. Its mechanism of antiviral activity has been attributed to its ability to bind to the high mannose oligosaccharides situated on the viral glycoprotein gp120 and possibly gp41 envelopes, thereby preventing the virus from fusing and penetrating host cells. CV-N has been shown to be nontoxic to tissue culture cells at concentrations much higher than that required for its anti-HIV activity [7]. Recombinant CV-N has been produced in *Escherichia coli* and has been structurally characterized using nuclear magnetic resonance spectroscopy and X-ray crystallography. Researchers have attempted to formulate CV-N as a microbicide and a multipurpose preventive technology [8]. Cell culture studies have consistently demonstrated the efficacy of Cyanovirin-N (CV-N) against HIV-1, HSV-2, and HPV at nanomolar concentrations (1–10 nM; ~0.011–0.11 μg/mL) [9–11]. In contrast, animal studies have employed significantly higher concentrations—ranging from 100 μg/mL to 2 mg/mL—without causing toxicity to vaginal epithelial tissue [12,13]. For this study, formulation concentration of CV-N 0.0005% (5 μg/mL) was used and thus justified, as it lies above the antiviral EC_{50} and well below the toxicity threshold, supporting both safety and efficacy in a multipurpose vaginal formulation. Moreover, the versatililty of hydrogels ensures concentrations adjustment by volume. Tenofovir Disoproxil Fumarate, chemically called 9-[[R]-2[[bis[[[isopropoxycarbonyl]oxy] methoxy] phosphonyl] methoxy] propyl] adenine fumarate is a nucleotide reverse transcriptase inhibitor clinically used with other antiretroviral for management of HIV infection. Abdool Karim et al., has demonstrated the efficacy of Tenofovir 1% in the management of HIV and Herpes simplex virus (HSV-2) with a success rate of 39% and 54% respectively in human subjects [14]. Nevertheless, resistance is highly likely with the use of a single antiviral. A synergistic approach may be necessary to improve outcomes.

Response surface methodology (RSM) is a commonly used statistical design that has been employed for statistical control of formulation design and formulation process to ensure development and optimization of production parameters through the control of desired response. There are two types of RSM, central composite design (CCD) and Box-Behnken design (BBD), CCD has been used in sequential experimentation while BBD has been used when fewer design points are required [15]. Artificial neural networks (ANNs), initially conceptualized in the 1960s, have advanced significantly since the 1980s alongside developments in computing. They have been widely applied in pharmaceutical sciences, particularly in optimizing drug formulations and manufacturing processes. ANNs excel at identifying complex, non-linear relationships in data, making them powerful tools for predictive modeling. When integrated with response surface methodology (RSM), which efficiently evaluates relationships between formulation variables, ANNs enhance optimization by improving accuracy, reducing experimental trials, and ensuring reliable predictions of critical quality attributes. This synergy streamlines pharmaceutical development, leading to high-quality, effective, and safe drug delivery systems with optimized therapeutic outcomes [16].

Currently, and to the best of our knowledge, no scientific study aimed at co-formulation of TNF and CV-N in form of a gel for multipurpose prevention strategies exists. The optimization process carried out in this study is vital for fine tuning the input factors (concentrations of the mucoadhesive polymer and crosslinker). The optimization process via ANN and BBD is also necessary for maximizing the TNF and CV-N gel formulation characteristics (flux, muco-adhesiveness and release). It also maximizes the efficacy of TNF/CV-N hydrogel and minimizes toxicity. The aim of this study is to optimize the hydrogel formulation of TNF boosted with CV-N through the establishment of ideal experimental conditions for co-formulation. This will foster optimum flux, adequate release of the active drug from its drug delivery system and muco-adhesiveness. This cutting-edge formulation promises effective prophylaxis of HIV, HSV and HPV.

2. Materials and methods

2.1. Materials

The following reagents were obtained commercially from the companies mentioned in the brackets. Tenofovir disoproxil fumarate (Energy Chemical Ltd), calcium chloride anhydrous (Klincent Laboratory, Mumbai). Polyethylene glycol (PEG) 2000, periodic acid (Maclin Pharmaceuticals). Sodium carboxymethyl cellulose (MW 700,000 Da), glycerin, methylparaben, propylparaben, bovine serum albumin (BSA), mucin, disodium hydrogen phosphate, potassium dihydrogen phosphate, sodium chloride, sodium chloride, potassium hydroxide, calcium hydroxide, lactic acid acetic acid urea, glucose and Schiff's reagent (Merck Specialities Pvt Ltd). TZM-bl cells ARP-8129 (BEI Resources, USA), MTT [3-[4,5-dimethylthiazol-2-yl]-2,5-diphenyl tetrazolium bromide](Thermofisher scientific, USA). Cyanovirin-N was purified at Bhabha Atomic Research Centre, Mumbai, India as described by Agarwal et al. [8].

2.2. Preparation and characterization of stable hydrogel formulation

Hydrogel formulations were prepared as illustrated in Table 1. Sodium carboxylmethyl cellulose NaCMC (at a concentration of 2–4% w/v) was dissolved in distilled water using a magnetic stirrer. Calcium chloride 0.1–1% was weighed and dissolved in distilled water. Tenofovir TNF

Table 1
Hydrogel formulations using NaCMC as polymer and calcium chloride as crosslinking agent.

INGREDIENTS	A	B	C	D	E	F	G	H
CV-N [% w/v]	0.0005	0.0005	0.0005	0.0005	0.0005	0.0005	0.0005	0.0005
Tenofovir [% w/v]	1	1	1	1	1	1	1	1
NaCMC [% w/v]	2	4	6	8	4	4.5	5	5.5
PEG [% w/v]	5	5	5	5	2	3	4	5
Glycerol [% w/v]	1	1	1	1	1	1	1	1
Propyl paraben [%w/v]	0.05	0.05	0.05	0.05	0.05	0.05	0.05	0.05
Methyl paraben [%w/v]	0.05	0.05	0.05	0.05	0.05	0.05	0.05	0.05
Calcium chloride [%w/v]	0.1	0.5	0.8	1	0.1	0.5	0.8	1
Dil HCl to pH 4.5	q. s	q. s	q. s	q. s	q. s	q. s	q. s	q. s
Distilled water to (mL)	100	100	100	100	100	100	100	100

(1g), dissolved in an aqueous solution of 5% PEG and 0.5 mg Cyanovirin-N in Phosphate Buffered saline (PBS) were added to the mixture and stirred until fully dispersed. The prepared calcium chloride solution was added and stirred for crosslinking. In a separate container, both methyl and propyl paraben (0.05 g) were dissolved in distilled water and slowly added to the mixture while stirring continuously. Glycerol (1 ml) was added to the mixture and stirred until hydrogel with a uniform consistency was formed. The pH was adjusted to 4.5 by addition of dilute hydrochloric acid (HCl). The final volume of hydrogel was 100 ml. The prepared hydrogel formulations were stored in clean glass containers.

2.3. Design of experiment

The experimental design for hydrogel production involved utilizing a Box-Behnken design (BBD) incorporating three factors representing the input variables: the concentration of $CaCl_2$, NaCMC, and PEG2000. The selection of the BBD was based on its advantageous characteristics, such as the reduction in the number of experimental runs, minimization of experimental errors through the distribution of the design points, capability to accommodate quadratic response surfaces, statistical efficiency in estimating model parameters, and satisfactory interpolation properties [17]. The design matrix was created using the Python library (PyDoE2) utilizing the inputs outlined in Table 2, which were established following preliminary experiments. Hydrogel formulations were prepared and the percent mucoadhesion, cumulative release and flux of the formulations were determined.

2.4. Artificial neural network modelling

The data generated from BBD was utilized to develop an Artificial Neural Network (ANN) model for the development of the hydrogel formulation. In this study, a feed-forward neural network architecture was employed. The hidden layer of the neural network comprises a group of neurons responsible for predicting the output response (y) based on the provided input features (x). The prediction involved using Equation (1) to compute a linear combination (z) of the input features (x_i) using corresponding biases (b) and weights (w_i). A critical aspect of the ANN modeling process is the activation function selection, which fundamentally influences the mapping of inputs to outputs. As a result, several activation functions, including rectified exponential linear unit (ReLU), leaky rectified linear unit (Leaky ReLU), and scaled exponential linear unit (SELU) were evaluated to identify the most appropriate option [18].

Table 2
Range of values for hydrogel formulation experiments.

Variables	Symbol	Coded and actual levels		
		−1	0	1
$CaCl_2$	X_1	0.1	0.55	1.0
NaCMC	X_2	4.0	4.50	5.0
PEG 2000	X_4	2.0	3.50	5.0

$$z = \sum_{i=1}^{n} x_i w_i + b \qquad \text{[Equation1]}$$

The ANN model underwent a training process that iteratively adjusts the model weights to minimize the model loss (ℓ), employing the root mean square error (RMSE) as a metric [Equation (2)]. This was accomplished through the utilization of a gradient descent method that updates the weights according to the model loss and is scaled using the learning rate (λ) as shown in Equation (3). The hyperparameters of the ANN were tuned using a grid search cross-validation (GridSearchCV).

$$\ell = \sqrt{\frac{1}{n}\sum_{i=1}^{n}(y_i - \hat{y}_i)^2} \qquad \text{[Equation 2]}$$

$$w_{t+1} = w_t - \lambda \frac{\partial \ell}{\partial w_t} \qquad \text{[Equation 3]}$$

where y_i and $\hat{y}_i$ is the experimental observation and model prediction, respectively.

All the procedures carried out during the development of the ANN model were implemented in Python 3.7.5 utilizing the TensorFlow library 2.4.0 with Jupyter as the integrated development environment (IDE). NumPy version 1.17.0 was employed for numerical analysis, and data visualization was carried out using Matplotlib (version 3.5). An HP EliteBook featuring an Intel Core i5 processor (1.9 GHz speed, 16 GB RAM, Windows 10) was utilized to execute all the codes. A 3-fold cross-validation was performed using the hydrogel formulation dataset, which was divided into an 80:20 train-test split, allocating 80 percent of the data for model training and the remaining 20 percent for evaluating their performance. Cross-validation was conducted on the complete training set, while testing was executed using a dedicated test dataset that was not exposed to the models during the training phase. This approach was adopted to mitigate the risk of overfitting, thereby enhancing the model's capacity to generalize effectively.

2.5. Assessment of ANN model fit

Statistical measures of model fit, including the coefficient of determination (R^2), root mean square error (RMSE), and standard error of prediction (SEP), were utilized to evaluate the level of fit of the ANN model with the experimental data, as depicted in Equations (4)–(6). Ideally, the R^2 value should approach one, representing a perfect fit between the experimental results and mode predictions. In practice, an R^2 value of at least 0.8 is considered indicative of an acceptable agreement between predicted and experimental results. Conversely, the error metrics (RMSE and SEP) should be minimized to signify a closer correspondence between the model predictions and the experimental observations [19].

$$R2 = 1 - \sum\_[i=1]\hat{n}[x\_[a,i] - x\_[p,i]\ ]\ 2/\ \sum\_[i=1]\hat{n}[x\_[p,i] - x\_[a,ave]\ ]\ \hat{2} \qquad \text{[Equation 4]}$$

$$RMSE = \sqrt{\left[1 / n \sum\_[i=1]\hat{n}\left[x\_[p,i] - x\_[a,i]\right]\hat{2}\right]} \quad \text{[Equation 5]}$$

$$SEP = RMSE / x\_[a,ave] \times 100 \quad \text{[Equation 6]}$$

In Equations (4)–(6), n is the number of experimental runs, $x\_[p,i]$ is the predicted value, $x\_[a,i]$ is the experimental values, and $x\_[a,ave]$ is the average of the experimental values.

2.6. Optimization of hydrogel formulation

In this study, manta ray foraging optimization (MRFO) was utilized. The manta ray foraging optimization is a nature-inspired swarm optimization algorithm that simulates the foraging behavior of manta rays during their search for food [20]. The algorithm replicates the natural foraging strategies of manta rays, including chain, cyclone, and somersault behaviors. In the chain foraging strategy, a group of manta rays identifies and moves in a chain-like formation toward a potential food source, maximizing overall feeding success to ensure that any missed food is quickly detected by the next member of the group. Subsequently, in the cyclone foraging approach, which typically follows the chain foraging, manta rays spiral towards their food while maintaining the foraging chain, with each member simultaneously advancing towards the target food. During the somersault phase, the food serves as a pivot in the search space, and the manta rays continuously maneuver around it, adjusting their positions until the optimal position is achieved. Equations (7), (8) and (10) show the mathematical representations of the chain, cyclone, and somersault foraging phases respectively.

$$x_i^d[t+1] = \begin{cases} x_i^d[t] + (r+\alpha)\left(x_{best}^d[t] - x_i^d[t]\right) & i = 1 \\ x_i^d[t] + r\left(x_{i-1}^d[t] - x_i^d[t]\right) + \alpha\left(x_{best}^d[t] - x_i^d[t]\right) & i = 2, 3, \ldots N \end{cases} \quad \text{[Equation 7]}$$

where x_i^d, x_{best}^d, r (0, 1) and α represent the position of the i^{th} individual in the d^{th} dimension, the best solution in the d^{th} dimension, a random vector, and weight coefficient respectively

$$x_i^d[t+1] = \begin{cases} x_{rand}^d[t] + (r+\beta)\left(x_{rand}^d[t] - x_i^d[t]\right) & i = 1 \\ x_{rand}^d[t] + r\left(x_{i-1}^d[t] - x_i^d[t]\right) + \beta\left(x_{rand}^d[t] - x_i^d[t]\right) & i = 2, 3, \ldots N \end{cases} \quad \text{[Equation 8]}$$

$$\beta = 2e^{r_1 \frac{T-t+1}{T}} sin\ 2\pi r_1 \quad \text{[Equation 9]}$$

Where x_{rand}^d, β, T and r_1 (0, 1) represent a vector showing the random position within the search space, weight coefficient, maximum number of iterations, and random vector

$$x_i^d[t+1] = x_i^d[t] + S\left(r_2 \times x_{best}^d[t] - r_3 \times x_i^d[t]\right) \quad \text{[Equation 10]}$$

where S represents the somersault factor while r_2 (0, 1) and r_3 (0, 1) represent vectors showing the random position within the search space.

2.7. Preparation of optimized hydrogel and characterization

The optimized hydrogel formulation was prepared as illustrated in Table 3. The prepared hydrogel was characterized. Percent release and flux of tenofovir as well as percent muco-adhesion were determined.

2.7.1. Scanning electron microscopy of tenofovir boosted CV-N hydrogel

Scanning electron microscopy (SEM) was used for the surface and structural characterization of the hydrogel. A Leica DM 6000 microscope was used and the images taken at × 500, × 1000 and × 1500 magnification at room temperature. A thin section of the hydrogel was fixed with 2.5% glutaraldehyde in phosphate-buffered saline (PBS), dehydrated with ethanol and dried. The dried hydrogel was mounted on the SEM stub with the use of carbon adhesive tape. The SEM was carried out in low vacuum mode at a voltage of 30.00 kV and a working distance of 12.3 mm. The CBS (Backscattered Electron Detector) was used to capture compositional contrast. Images were acquired in both bright-field and dark-field modes, allowing detailed visualization of the hydrogel matrix and embedded particles. Adjustments to focus, contrast, and brightness were made to enhance image clarity and scale bar indicated.

Table 3
Optimized Hydrogel formulation.

INGREDIENTS	%w/v
CV-N	0.0005
Tenofovir	1
NaCMC	4
PEG2000	2
Glycerol	1
Propyl paraben	0.05
Methyl paraben	0.05
Calcium chloride	1
Distilled water to	100 Ml
Dil HCl to pH 4.5	q. s

2.7.2. Assessment of interaction using FTIR

The compatibility of TNF, CV-N, and other ingredients was evaluated using FTIR. The samples were scanned in the wave number range of 600–4000 cm^{-1}. The spectra of the individual drug ingredients were compared with that of the hydrogel formulations. The appearance or disappearance of peaks were noted to ascertain probable interactions, both physical and chemical [21].

2.7.3. Physicochemical evaluation

The prepared hydrogels were visually inspected for odor, color, phase separation and formation of precipitates and the presence of any clog. Hydrogels were also evaluated for the feel and external appearance.

2.7.4. Stability measurement

The pH, viscosity, homogeneity of the hydrogel was determined at scheduled time intervals (day 1, 18, 36, 48, 60, and 90) during a 3-month storage period at 5 ± 2 °C, 25 ± 2 °C/65 ± 5% RH and 40 ± 2 °C/75 ± 5% RH. Physical stability was also monitored for any visual instabilities, such as fusion and aggregation.

2.7.5. Osmolarity

The osmolarity was calculated by converting the concentration of each component to moles per liter (mol/L), adjusting for the Van't Hoff factor where applicable, and summing these values to get the total osmolarity in osmoles per liter (Osm/L).

2.7.6. X-ray diffraction

Structure and distribution of active drug in gel was elucidated by X-ray diffraction This technique was used to analyze the structural properties of the gel formulation and their interaction with the excipients [22].

2.7.7. Mucoadhesion test

Mucoadhesive test of the prepared hydrogels was measured with respect to mucin adsorption (porcine stomach type II) and periodic acid/Schiff colorimetric method [23]. The absorbance was measured at a wavelength of 555 nm and the mucin content calculated from the standard calibration curve. Each experiment was performed in triplicate with mucin adsorption calculated using: $\%\,MA = \frac{TMM-FM}{TMM}\ x\ 100$ [Equation (11)]

Where MA is Mucin Adsorption, TMM is Total mass of mucin and FM is free mucin.

2.7.8. In-vitro drug permeability and flux of tenofovir

The experiment was performed using the Franz® diffusion cells with an available diffusional cross-sectional area of 0.98 cm^2 on a 0.45 μm white girded Millipore® membrane (CAT. NO. HAWG047S6, LOT. NO. F0JB71372C). A pH 4.5 simulated vaginal fluid [SVF] was used as the receptor (kept at 37 ± 1 °C in a water bath) compartment of the Franz® diffusion cell and filled with 25 mL of SVF. The concentrations of the permeant at varying time lapses were measured with UV spectrophotometer at 260 nm. Measurements were taken in triplicate and a plot of concentration permeated against time plotted. The drug flux at a steady state (μg/cm^2/h) was calculated from the slope of the linear portion of the cumulative amount permeating the membrane [23].

2.7.9. In-vitro cytotoxicity of optimized hydrogel formulation

Cytotoxicity of hydrogel was evaluated using MTT cell proliferation assay. TZM-bl cells were seeded at the density of 10,000 to 12,000 cells/well in forty-eight well plate containing 100 μL of Dulbecco's Modified Eagle Medium and incubated with the hydrogel containing CV-N/TNF and CV-N pure sample for 48 h. The experiment was performed in quadruplicate. After a 48 h incubation period, 10 μL of MTT was added in each well in the dark and incubated at 37 °C for the formazon crystal formation. 4 h after incubation, the crystals were dissolved using isopropanol and the absorbance was read at 570 nm. Cell viability was assessed on days 1, 2, and 3 as per MTT method. The absorbance obtained for CV-N was compared to control cells (no treatment) [24].

2.7.10. HIV efficacy testing

The TZM-bl cells were seeded in 24-well plates to obtain an optical density corresponding to 2×10^5 cells in each well which would correspond to 60–80% confluency. The cells were treated with dilutions of the CV-N/TNF hydrogel, CV-N standard solution, TNF standard solution and nonoxynol-9 gel. The results of the treatment were compared with control (HIV-infected cells without antiretroviral treatment) and data obtained was plotted to obtain an HIV infectivity dose-response curve. All the experiments were performed in quadruplicates [25].

2.7.11. Safety assessment studies

The safety assessment study was carried out using a modified RVI test model. Healthy female adult naïve rabbits with weights around 2–5 kg, were purchased from Nomad Farms, Sango Ota, Ogun State, Nigeria. All animal tests were carried out in compliance with The National Institutes of Health guide for the care and use of laboratory animals and institutional guidelines approved in writing by Health Research Ethical Committee with approval number CMUL/HREC/012/23/1341. The rabbits were kept in a temperature-controlled facility (22 ± 2 °C) with relative humidity (40 ± 3%) and a 12-h light/dark cycle for at least one week before usage with unrestricted access to food and water. The ARRIVE guidelines were used for documenting the study. The rabbits were grouped into six groups containing two rabbits per group. Group F1 was treated with CV-N/TNF hydrogel formulation, group F2 was treated with 0.0005% CV-N in phosphate buffered saline (PBS), while group F3 was treated with 1% Tenofovir hydrogel, F4 consisted of rabbits treated with nonoxy-9 (N9) gel and a control group to access the influence of tweezers on the vagina (CON). Following 24 and 72 h of drug administration, the rabbits were humanely put to death by being exposed to carbon dioxide gas; no anesthetic was used during the procedure. The tissues from the vagina area were removed, sectioned into outer, middle and inner vagina then placed in sterile sample vials with 10% formalin in saline for histological analysis. The sections were stained with hematoxylin and eosin. They were viewed × 100 and photographed using a Leica DM 750 microscope and ICC HD 50 camera [23].

2.8. Statistical analysis

Data obtained were expressed as mean ± SD (standard deviation). ANOVA was used to test if there were significant differences in the data obtained. p values ≤ 0.05 were considered statistically significant.

3. Results and discussion

3.1. ANN model analysis

The ANN model was trained by tuning its respective hyperparameters and the results are shown in Table 4. The ANN model with its optimized hyperparameters was used to predict the three responses [mucoadhesion, flux and drug release] and the values are presented in Table 5 alongside the experimental data for comparison. The prediction accuracy was assessed using different statistical metrics as shown in Table 6. From the data in Tables 5, it can be observed that the model predictions were very close to the experimental observations, indicating minimal deviation between them and thus showing validity of the ANN model. This observation was also corroborated by the goodness of fit statistics presented in Table 6. The parity plots presented in Fig. 1 compare the predicted and actual results for the three responses. The clustering of data points around the 45° diagonal line in the parity plots indicates a satisfactory level of agreement between the experimental and model-predicted results, signifying minimal deviation between the two sets of values and thereby confirming the validity of the model [26].

3.2. Effect of input factors on the responses

To evaluate the individual and interactive effects of the input factors on mucoadhesion, flux, and drug release, one-way and two-way (depicted in Figs. 2–4) partial dependence plots (PDPs were produced. The generation of PDPs involves aligning all data points to assume the same feature value, allowing the partial dependence function to reflect the average prediction of the output. One of the primary advantages of utilizing PDPs is their intuitive nature, straightforward implementation, capacity to explicitly model a causal relationship between input factors and model outputs, and ability to elucidate the association between outputs and inputs regardless of the nature of the relationship. Additionally, PDPs are model-agnostic, meaning that they can be employed with any model [19].

Fig. 2A–C presents the one-way PDPs showing the influence of individual input factors on mucoadhesion. In Fig. 2A, the concentration of $CaCl_2$ displayed an almost linear effect on mucoadhesion, with lower values of $CaCl_2$ resulting in higher mucoadhesion values. This trend suggests that the concentration of $CaCl_2$ inversely affects the mucoadhesion, with lower concentrations promoting greater mucoadhesion. This observation could be attributed to the role of $CaCl_2$ in altering the rheological properties of the hydrogel, thereby affecting its adhesive characteristics to mucosal surfaces [27]. Reduction in the concentration of calcium chloride may increase mobility of hydrogel polymers, thereby promoting adherence to the mucosal surface. The ratio of the polymers

Table 4
Optimized values of hyperparameters for ANN model.

Hyperparameters	Final optimized value		
	Mucoadhesion (%)	Flux (g/cm^2/h)	Drug release (%)
layer 1 number of neurons	100	100	100
layer 2 number of neurons	400	400	400
layer 3 number of neurons	400	400	400
layer 4 number of neurons	400	400	400
layer 5 number of neurons	400	400	400
activation function (all layers)	ReLU	ReLU	ReLU
Alpha	0.1	0.5	1
model optimizer	Adam	Lbfgs	Lbfgs
random_state	42	42	8
R^2	0.9495	0.9801	0.9981

lbfgs = Limited-memory Broyden–Fletcher–Goldfarb–Shanno.

Table 5
Comparison of experimental results with ANN predicted results.

Run	Inputs			Responses					
				Mucoadhesion (%)		Flux (g/cm^2/h)		Cumm. drug release (μg/cm^2)	
	$CaCl_2$	NaCMC	PEG 2000	Experiment	Predicted	Experiment	Predicted	Experiment	Predicted
1	0.10	4.5	2.0	98.1	98.7	2767.5	2995.0	19379.5	19469.3
2	0.55	5.0	2.0	99.4	99.3	2900.7	2873.8	20962.3	20976.9
3	1.00	4.0	3.5	96.5	97.7	2291.0	2264.1	16623.3	16580.9
4	1.00	4.5	2.0	95.1	96.4	4319.3	4313.2	34528.1	34558.6
5	0.55	4.5	3.5	99.0	99.3	3534.4	3317.0	24464.8	25589.1
6	0.55	4.5	3.5	99.5	99.3	3735.4	3317.0	26359.9	25589.1
7	0.10	5.0	3.5	99.5	100.6	4319.3	4513.7	27986.0	27866.1
8	1.00	4.5	5.0	94.7	93.9	3131.9	3565.7	23786.7	24481.7
9	0.55	4.5	3.5	99.0	99.3	3111.0	3317.0	24203.8	25589.1
10	0.55	4.0	2.0	98.8	97.6	11272.0	11288.1	84599.1	84592.8
11	0.10	4.0	3.5	99.2	99.4	2929.3	3235.0	24153.3	24124.4
12	0.55	4.5	3.5	98.7	99.3	3634.7	3317.0	26669.0	25589.1
13	1.00	5.0	3.5	100.0	99.6	2777.4	3174.9	19404.4	19267.7
14	0.55	5.0	5.0	96.4	97.1	5061.0	4812.1	34984.1	34302.9
15	0.10	4.5	5.0	97.4	96.9	4524.6	4686.1	34629.2	35320.4
16	0.55	4.0	5.0	85.4	86.7	3695.1	3512.2	28334.2	27758.4
17	0.55	4.5	3.5	99.4	99.3	3838.2	3317.0	26248.6	25589.1

Table 6
Assessment of ANN model prediction accuracy for mucoadhesion, flux and drug release.

Parameter	Value		
	Mucoadhesion (%)	Flux (μg/cm^2/h)	Drug release (μg/cm^2)
R^2	0.9495	0.9801	0.9981
MSE	0.5744	75875.5325	422320.4533
RMSE	0.7579	275.4551	649.8619
AAD	0.6298	229.9533	478.3561
SEP	0.0064	0.6619	0.0627
MAE	0.6298	229.9533	478.3561

to crosslinker $CaCl_2$ is crucial to optimize mucoadhesiveness [28]. Overly high concentration of calcium chloride relative to the polymer concentrations may result in formation of stiffer gels, thereby reducing mucoadhesiveness of the formed hydrogel [29]. Moreover, hydrogels with low concentrations of calcium chloride tend to swell more readily when in contact with fluids present on mucosal surfaces, promoting better interaction with mucosal and enhancing mucoadhesion.

The concentration of NaCMC exhibited a positive influence on mucoadhesion, as indicated by the nearly linear increase in mucoadhesion values with increasing NaCMC concentration, as depicted in Fig. 2B. This observed trend suggests that higher concentrations of NaCMC contribute to enhanced mucoadhesive properties, possibly due to the increased interaction between NaCMC and mucosal surfaces, leading to improved adhesion [30]. Diffusion of the polymer chains into the loops or gaps in the glycoprotein network and the formation of new noncovalent bonds further promote mucoadhesion [31]. Furthermore, sodium carboxymethylcellulose possess the ability to form hydrogen bonds with the oligosaccharide chains of mucins with increasing mucoadhesiveness observed as the length of the polymer chains increases. The polymer chains are flexible enhancing penetration and entanglement of the polymers with the mucosal layer, hence increasing mucoadhesion [32]. The flexibility of the polymer chains can be affected by crosslinking reaction with an increase in crosslinker concentration resulting in decrease in mucoadhesion [33]. Furthermore, Fig. 2C shows the impact of PEG2000 on mucoadhesion, revealing an initial increase in mucoadhesion with increasing PEG2000 concentration, reaching a peak value of approximately 99% before declining as the concentration of PEG2000 exceeded 3.5 g/100 mL. This trend may be attributed to the role of PEG2000 in modifying the network structure and viscosity of the hydrogel, influencing its mucoadhesive properties [34]. PEG2000 may also promote hydration of the mucosa, thereby enhancing lubrication and mucoadhesion [35]. Extensive research needs to be carried out to further explore these interactions. Fig. 2D–F presents the two-way PDPs, elucidating the combined and interactive effects of the three inputs on mucoadhesion, flux, and drug release.

The figures indicate an important interaction between the inputs, highlighting their collective impact on the responses, thereby highlighting the complex interplay of $CaCl_2$, NaCMC, and PEG2000 in influencing mucoadhesion, flux, and drug release in the tenofovir-boosted Cyanovirin hydrogel formulation.

Fig. 3A presents a one-way PDP that illustrates the influence of $CaCl_2$ on the flux of a tenofovir-boosted recombinant Cyanovirin-N hydrogel formulation. The trend observed from the plot suggests that the presence

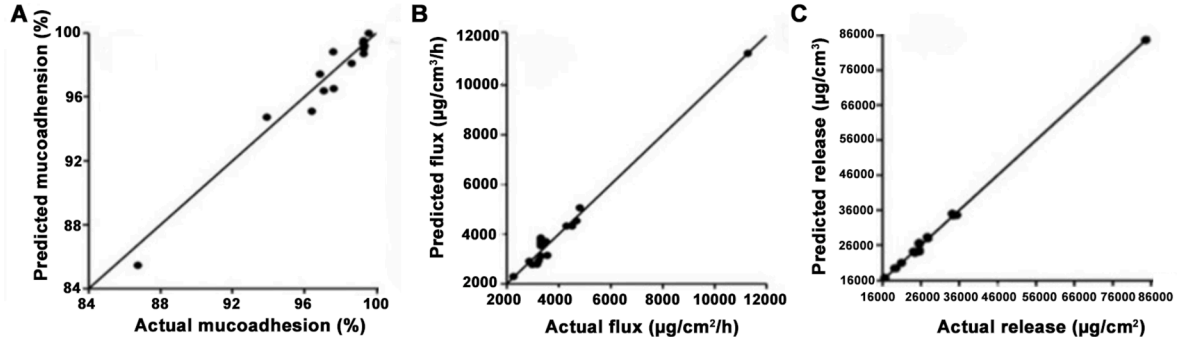

Fig. 1. Parity plot showing comparison of experimental and (A) predicted mucoadhesion (B) predicted flux and (C) predicted drug release.

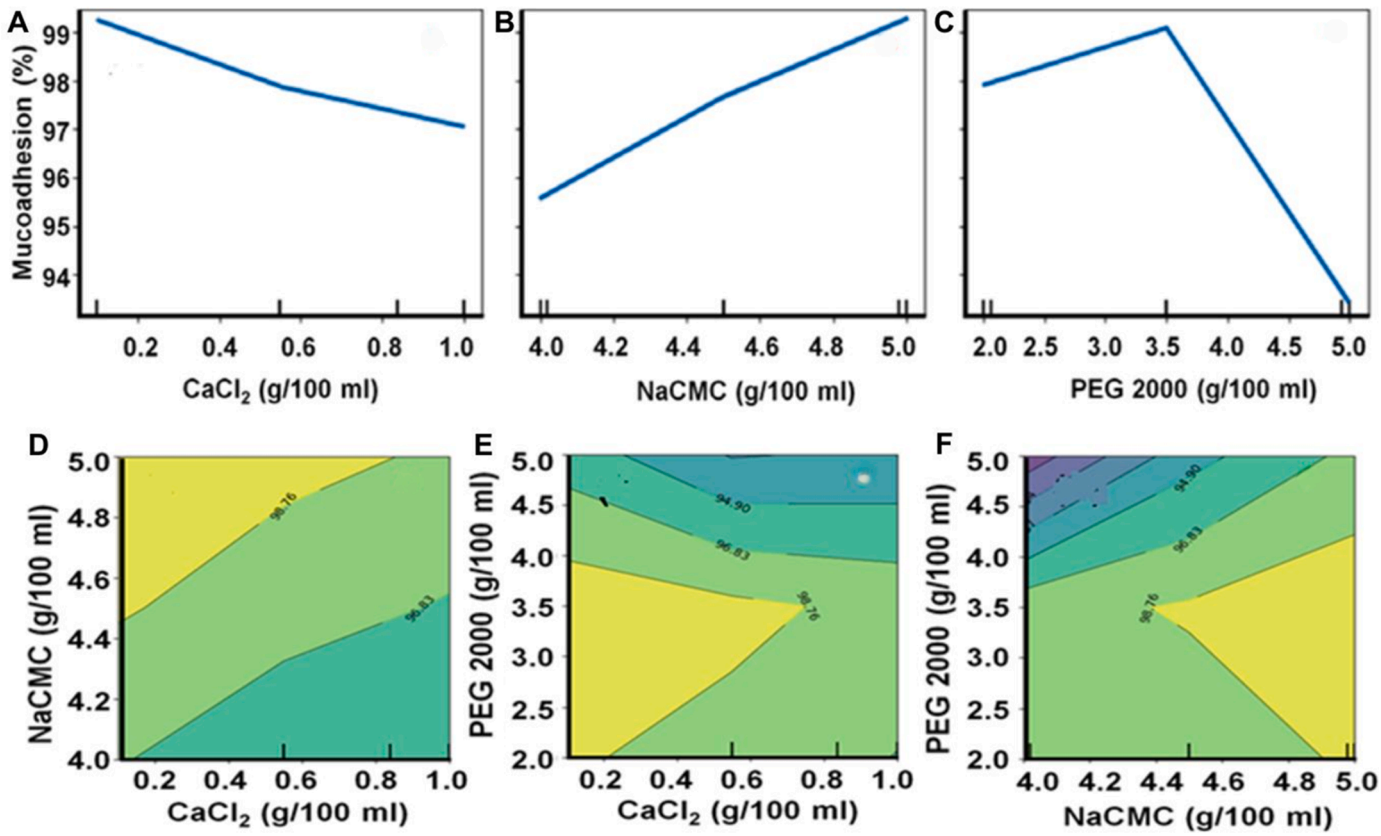

Fig. 2. A–F: One-way partial dependence plot showing the impact of (A) $CaCl_2$, (B) NaCMC, and (C) PEG2000 on muco-adhesion. Two-way partial dependence plot showing the impact of (D) $CaCl_2$ and NaCMC, (E) $CaCl_2$ and PEG2000 and (F) PEG2000 and NaCMC on muco-adhesion.

of $CaCl_2$ in the formulation has a minimal effect on the flux, indicating that the drug permeation rate through the hydrogel matrix is largely unaffected by the concentration of $CaCl_2$. This indicates that increased concentration of calcium chloride does not result in significant increase in crosslinking density. In general terms, increased crosslinking density results in high hydrogel density, slower drug release and flux. However, the trend observed in this hydrogel slightly differs with negligible influence of the crosslinker concentration on flux. This might imply the poor interaction of tenofovir with the crosslinker and the hydrogel matrix. Moreover, the initial elastic modulus in hydrogels may be impacted by swelling. Swollen hydrogels with high water content may readily interact with biological medium due to high mucosa adhesion [36]. The presence of diffusion pathways in the hydrogel formulation may also be unaffected by the concentration of calcium chloride, hence diffusion of tenofovir will remain unaffected and consequently its flux [37]. In contrast, the concentrations of NaCMC and PEG2000 exerted a more pronounced influence on the flux. As depicted in Fig. 3B and C, an initial decrease in flux was evident with an increase in the concentration of NaCMC [from 4 to 4.5 g/100 mL] and PEG2000 (from 2 to 3.5 g/100 mL). This decrease may be attributed to the increased mechanical strength and viscosity of the hydrogel matrix due to the higher polymer concentration, potentially impeding drug diffusion [38]. However, a subsequent increase in flux is observed, of which reason could be excessively high concentration of PEG may cause degradation of the hydrogel [39]. Fig. 3D–F shows two-way PDPs that depict the interactive effect of $CaCl_2$, NaCMC, and PEG2000 on the flux. The interplay between these components in the formulation may lead to complex changes in the physicochemical properties of the hydrogel, thereby influencing drug release behavior and flux [40]. Further investigation might be necessary to elucidate the precise mechanisms underlying these observations. Microstructural analysis, rheological studies, crosslinking density analysis, Fourier-transform infrared spectroscopy (FTIR) can provide in-depth insight on the interactive effects of calcium chloride, NaCMC, and PEG2000 on flux [41].

Fig. 4A depicts the impact of $CaCl_2$ on the drug release of the hydrogel formulation. The observed trend indicates that an increase in the concentration of $CaCl_2$ from 0.1 to 0.6 g/100 mL does not significantly impact the level of drug release. However, a decline in drug release was observed when the $CaCl_2$ concentration was increased beyond 0.6 g/100 mL. This decline in drug release could be attributed to the potential formation of a more rigid hydrogel network due to increased ionic cross-linking, which may impede drug release [42]. The effects of NaCMC and PEG2000 on drug release mirrored their impact on flux, as illustrated in Fig. 4B and C. An increase in the NaCMC concentration from 4 to 4.5 g/100 mL resulted in a reduction in drug release (Fig. 4B). However, this trend reversed when the NaCMC concentration increased beyond 4.5 g/100 mL. Similarly, Fig. 4C shows that an increase in the PEG2000 concentration from 2 to 3.5 g/100 mL leads to a decrease in drug release, but this trend reversed when the PEG2000 concentration was increased above 3.5 g/100 mL. These observations could be attributed to the intricate interplay between the viscosity of the hydrogel matrix and the solubility of the drug. At higher concentrations of NaCMC and PEG2000, the increased viscosity of the hydrogel matrix may initially impede drug release [43]. However, beyond a certain concentration, the enhanced solubility and dispersibility of the drug within the hydrogel matrix may facilitate increased drug release. The initial decrease in drug release at higher polymer concentrations is due to the increased viscosity of the hydrogel matrix, which hinders drug diffusion. However, once the polymer concentration reaches a certain level, the enhanced solubility and dispersibility of the drug within the hydrogel matrix can overcome this barrier, leading to increased drug release [44].

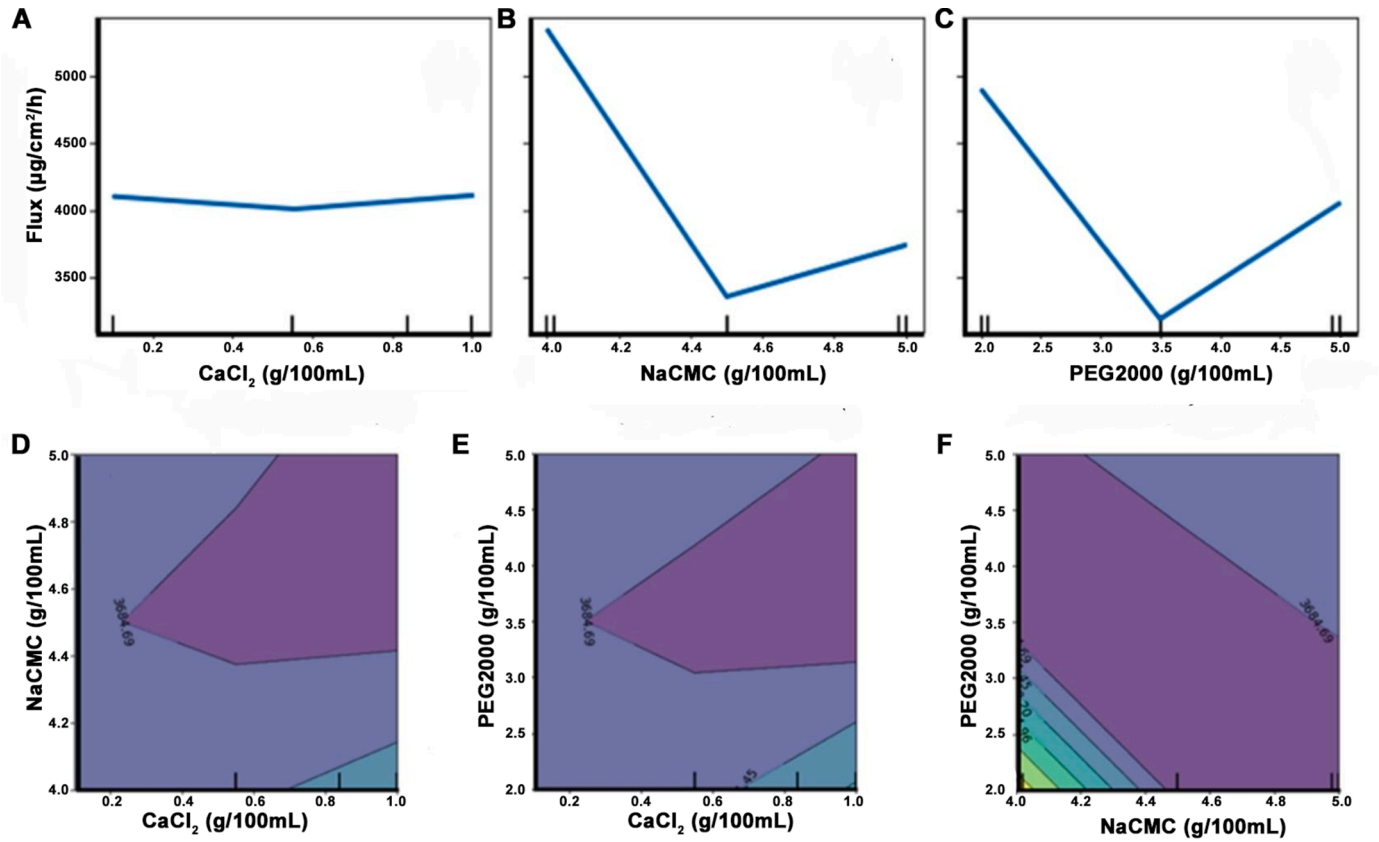

Fig. 3. A–F: One-way partial dependence plot showing the impact of $CaCl_2$ (A), NaCMC (B), and PEG2000 (C), on flux. Two-way partial dependence plot showing the impact of $CaCl_2$ and NaCMC (D), $CaCl_2$ and PEG2000 (E) and PEG2000 and NaCMC (F) on flux.

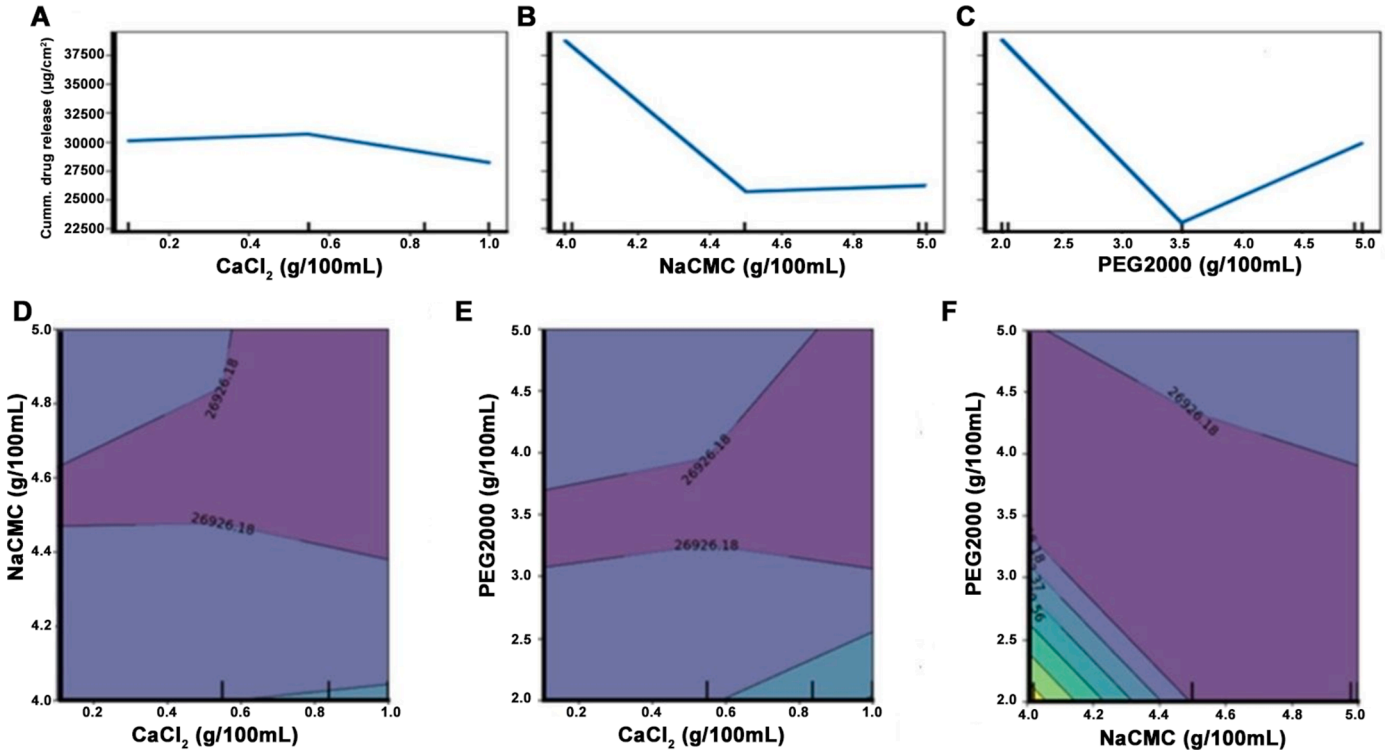

Fig. 4. (A–F): One-way partial dependence plot showing the impact of $CaCl_2$ (A), NaCMC (B), and PEG2000(C) on cumulative drug release. A two-way partial dependence plot showing the impact of $CaCl_2$ and NaCMC (D), $CaCl_2$ and PEG2000 (E) PEG2000 and NaCMC (F) on cumulative drug release.

3.3. Optimization of input factors and responses

This study deployed a nature-inspired optimization algorithm, MRFO, to optimize the hydrogel formulation. Table 7 presents the optimized hyperparameters of the MRFO algorithm which was used to obtain the optimized formulation. The maximum mucoadhesion, flux and drug release predicted by the MRFO algorithm were 96.1%, 9808.8 μg/cm^2/h and 119,581.6 μg/cm^2 respectively which is close to the experimental value of 96.3%, 9806 μg/cm^2/h and 119,205.6 μg/cm^2 obtained. The high mucoadhesiveness is desirable for an optimum drug release system, the high flux ensures delivery of the incorporated therapeutically active moiety reaches the desired site, whereas the drug release is essential to ascertain therapeutic effectiveness and optimum dosage regimen. The corresponding values of $CaCl_2$, NaCMC, and PEG2000 concentration were 1, 4 and 2 g/100 mL respectively as shown in Table 8. In order to validate this optimized conditions, triplicate experiments were carried out at these optimum values and the average values of mucoadhesion, flux and drug release obtained from the three experiments were very close to those predicted by the MRFO algorithm.

3.4. Characterization of optimized hydrogel

The hydrogel formulation was off-white and of great gel consistency with no lumps. The odor was agreeable; the hydrogel was easily spread and easy to wash off with water. The pH of the hydrogel formulation was 4.50 ± 0.017 consistent with the vaginal pH, while viscosity at 10 rpm was 275600 ± 0.65. Stability studies carried out at 25 ± 2 °C/65 ± 5% RH and 40 ± 2 °C/75 ± 5% RH for a period of 3 months revealed a stable hydrogel formulation as evident by the consistency in the pH, viscosity and physical appearance over a period of three months. The hydrogel maintained its rheological properties under both storage conditions. The ease of application and washing off of the hydrogel formulation as well as its viscosity that allows adequate retention in the vagina has implication for end user acceptance, adherence and efficacy. Moreover, this makes the formulation discreet, allowing end-user's total control in administration. This is in compliance with a study carried out by Holt et al., emphasizing a high level of end-user preference for female controlled, discreet, long-acting products for use as MPTs [2].

3.4.1. Osmolarity

The osmolarity value was calculated to be approximately 472 mOsm/kg (see supplementary files). Vaginal formulations need to be isotonic or nearly isotonic to avoid irritation or discomfort. The normal osmolarity of vaginal fluids is around 290–310 mOsm/kg. The World Health Organization (WHO) stipulates that vaginal gels with an osmolality below 1200 mOsm/kg are acceptable. A formulation with an osmolarity of 450 mOsm/L or 472 mOsm/kg is slightly hypertonic compared to vaginal fluids and can pose a risk to vaginal tissue, causing discomfort, vaginal irritation and affect end user acceptance. Hyperosmolal lubricants such as spermicide nonoxynol-9 (N-9) can compromise the integrity of the human colorectal and vagina epithelium by causing exfoliation and weakening its barrier function. These harmful effects may increase vulnerability to STIs such as HIV and Herpes Simplex Virus (HSV). Hypertonic formulations can sometimes enhance drug absorption by creating an osmotic gradient, which draws water into the vaginal lumen. However, this effect needs to be balanced against potential irritation [45]. For future formulations, the concentration of some components that can increase osmolarity such as glycerol might be reduced or substituted with hyaluronic acid. Isotonic agents such as sodium chloride might be added to lower the osmolarity closer to physiological levels [46]. While the estimated osmolarity provides a useful estimate, the actual measured osmolarity is often lower due to the three-dimensional network of the hydrogel which can encapsulate solutes, preventing them from contributing fully to the osmolarity. Some solutes may be trapped within the gel matrix and not fully available in the free water phase. Chemical interactions between the solutes and the hydrogel matrix may reduce the number of free particles in solution. For example, polymers like NaCMC can form hydrogen bonds or ionic interactions with other solutes, decreasing their free concentration.

Table 7
Optimized values of hyperparameters for MRFO.

Hyperparameters	Final optimized value
Somersault range	2.5
Epoch	150
Population size	100

Table 8
Optimization results for hydrogel formulation.

Variables	Optimized values
$CaCl_2$ (g/100 mL)	1.0
NaCMC (g/100 mL)	4.0
PEG2000 (g/100 mL)	2.0
Predicted mucoadhesion (%)	96.1
Actual mucoadhesion (%)	96.3
Predicted flux (μg/cm^2/h)	9808.8
Actual flux [(g/cm^2/hr)	9806
Predicted drug release (μg/cm^2)	119,581.6
Actual drug release (μg/cm^2)	119,205.6

3.4.2. Fourier transmission infra-red spectroscopy

The FTIR spectra for CN-V, Na CMC, PEG2000, Tenofovir, calcium chloride and the CV-N/TNF hydrogel formulation provide valuable insights into the functional groups present in chemically active moieties as well as chemical interactions when these moieties are formulated [47]. CV-N spectrum revealed broad peak suggestive of hydroxyl/amine functional group O-H/N-H at around 3300 cm^{-1}. This is common in proteins. Other peaks observed around 1650 cm^{-1} and 1550 cm^{-1} can be attributed to amide I (C=O stretching) and amide II (N-H bending) bands, respectively. Sodium carboxymethylcellulose spectrum consisted of broad peak around 3400 cm^{-1} indicating hydroxyl [O-H] stretching vibrations. Peaks observed at 1600 cm^{-1}, 1420 cm^{-1} and 1050 cm^{-1}can be attributed to carboxylate (COO^-) asymmetric stretching, COO^- symmetric stretching and C-O-C stretching. The PEG 2000 Spectrum revealed O-H stretching vibrations, C-H stretching and C-O-C stretching vibrations at 3450 cm^{-1}, 2900 cm^{-1} and 1100 cm^{-1} respectively. The spectrum for tenofovir indicated peaks suggesting phosphate group at around 1100-1200 cm^{-1} as well as O-H (3200 cm^{-1}), C-O (1600 cm^{-1}) and N-H (3400 cm^{-1}) bonds. The CV-N/TNF hydrogel spectrum reveals combined spectra of CV-N, NaCMC, PEG 2000, calcium chloride and TNF with peaks attributed to individual component of the hydrogel duly represented on the spectrum as highlighted in Fig. 5. However, broadening of the peaks attributed to calcium chloride, tenofovir and sodium carboxyl methylcellulose was observed (wavelength below 3000 cm^{-1}) alluding to the successful crosslinking of tenofovir with the polymer by calcium chloride likely by weak forces of interaction or physical entrapment. The physical entanglement of polymer chains (NaCMC and PEG 2000) likely contributes to the hydrogel's structure with possible weak hydrogen and van der Waals forces of interactions between the polymers and the active moieties (CV-N and TNF). This force ensures stabilization of the hydrogel matrix. The characteristic peaks of CV-N and TNF present in the hydrogel spectrum confirms the successful incorporation of these components into the hydrogel matrix.

3.4.3. Scanning electron microscopy of tenofovir boosted CV-N hydrogel

The SEM images [Fig. 6A–C] show dispersed drug particles of tenofovir and CV-N within the hydrogel matrix at varying magnification. The distinct, bright, square or rectangular particles dispersed throughout the hydrogel matrix are suggestive of crystalline forms of the crosslinker calcium chloride. The unbounded calcium chloride indicates a supersaturation effect alluded to a high concentration used when compared to

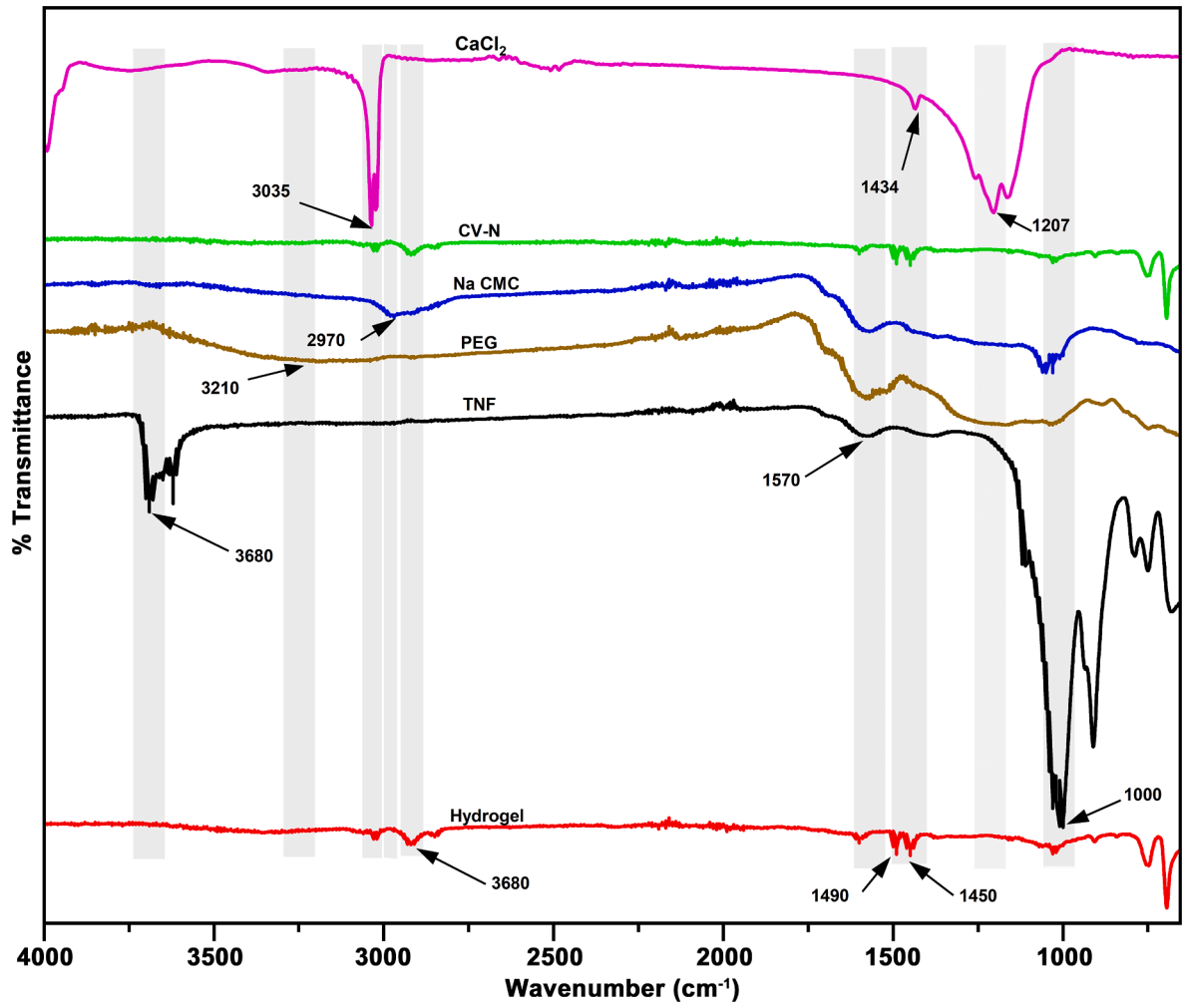

Fig. 5. FTIR of optimized hydrogel formulation and formulation ingredients.

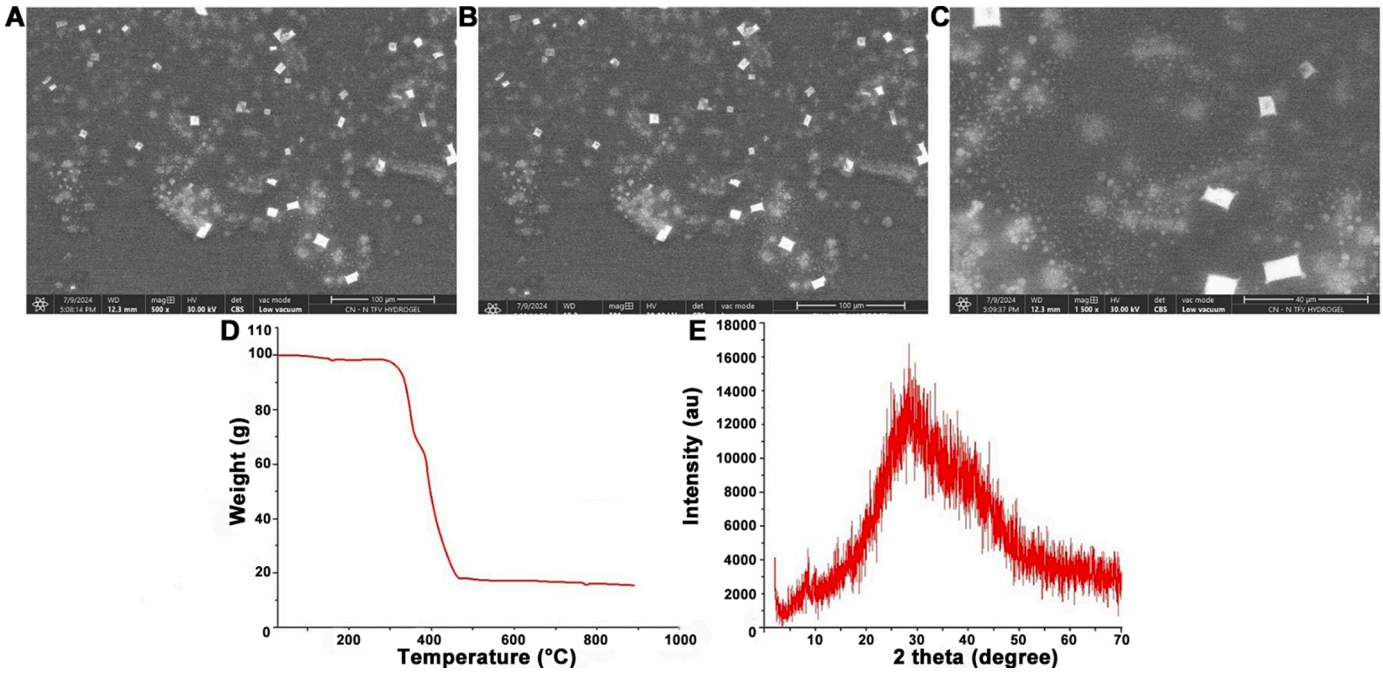

Fig. 6. A. SEM images of TNF/CV-N hydrogel formulation at 500x; B. SEM images of TNF/CV-N hydrogel formulation at 1000x; C. SEM images of TNF/CV-N hydrogel formulation at 1500x; D. TGA of optimized hydrogel; E. XRD of optimized hydrogel.

the concentration of the polymers. Nonetheless, this did not impact the physicochemical characteristics of the hydrogel. The hydrogel particles were uniform in shape and the homogeneity of the porous hydrogel network can be observed in the images. While the particles are visible, particle size measurements of the hydrogel required additional imaging software Image J, with the × 1500 magnification images used (supplementary file). Thirty particles were selected and the average particle size determined. The diameter of the hydrogel pores measured via Image J was 1200 ± 0.46 nm.

3.4.4. Thermogravimetric analysis

The heat stability of the optimized hydrogel formulation was investigated by TGA (Fig. 6D). The initial decomposition observed at 300 ^{o}C was due to loss of water and breakdown of the hydrogel polymer matrix, with 80% of the hydrogel mass degraded. The huge loss in mass demonstrates a high-water content of the hydrogel. This is in-line with published literature by Kumar et al., on thermal degradation of sodium carboxyl methylcellulose hydrogel formulations [48]. Subsequent decomposition observed beyond 300 ^{o}C is due to complete degradation of the hydrogel polymer as well as loss of crosslinkers, side-chains and other additives [49]. The high temperature observed for the initial degradation supports the stability of the hydrogel matrix.

3.4.5. X-ray diffraction (XRD)

The XRD of the optimized hydrogel (Fig. 6E) highlighted the amorphous nature of the hydrogel as illustrated by the broad peaks detected. The presence of well-defined peaks in the XRD spectrum of formulations typically illustrates the presence of crystalline planes as described by Saad et al. [50]. This was however not observed in spectrum of the optimized hydrogel formulation despite the presence of tenofovir, a crystalline moiety as described by Hotter et al. [51]. The amorphous nature of tenofovir in the hydrogel highlighted an interaction between the polymer and the incorporated tenofovir and could have implications enhancing its solubility, release and bioavailability. The incorporated CV-N was detected in an amorphous state in the hydrogel, although it has been reported to form crystals at low pH and in 26% isopropanol due to domain swapping of the two monomers of this moiety [52].

3.4.6. Anti-HIV efficacy studies

The anti-HIV efficacy studies carried out assessed the effect of the optimized hydrogel formulation, CV-N solution and nonoxynol-9 on the TZM-bl cells to establish the efficacy of these formulations against HIV cells. The response with varying concentrations was measured. To ascertain the minimum concentration with no HIV infectivity, dilutions of the hydrogels, N-9, CV-N and TNF standard solutions that resulted in zero HIV infectivity was determined (Fig. 7B). The TZM-bl cells were exposed to the optimized hydrogel, CV-N, TNF and nonoxynol-9 which was chosen as a placebo as it does not have activity against the HIV virus but is an effective spermicide with favorable safety profile [53]. The minimum concentration where zero HIV infectivity was observed for the optimized hydrogel was CV-N 0.05 μg and TNF 100 μg, whereas similar trend was observed for CV-N standard solution at 200 μg and TNF standard solution 1000 μg. The increased HIV inhibition at lower CV-N/TNF hydrogel concentration can be attributed to the combined antiretroviral efficacy of CV-N and TNF co-formulated in the optimized hydrogel alluding to the synergism of both moieties against HIV infection. This demonstrates the efficacy of the hydrogel formulation for HIV prophylaxis at low dosages, minimizing toxicity and the risk of resistance development. In contrast, nonoxynol-9 showed no reduction in HIV infectivity even at higher concentrations, highlighting its lack of potency against the virus.

3.4.7. In-vitro cytotoxicity assay

The *in vitro* cytotoxicity of the optimized hydrogel formulation using the MTT cytotoxicity assay to TZM-bl cells was compared with that of Cyanovirin-N solution as depicted in Fig. 7A. The MTT assay is a widely used method to assess cell viability, proliferation, and cytotoxicity. It involves the use of a yellow tetrazolium salt called MTT [3-(4,5-dimethylthiazol-2-yl)-2,5-diphenyl tetrazolium bromide]. The MTT is converted to a purple formazan product which is insoluble by living cells' mitochondria activity. The concentration of formed formazan is proportional to viable cell number [54]. The percent cell viability after exposure of the TZM-bl cells to the optimized hydrogel formulation and CV-N standard was measured for 72 h [Fig. 7B]. Both the hydrogel and the CV-N standard solution assayed at CV-N 5 μg/mL exhibited high percent cell viability for the 72 h assay period. However, the optimized CV-N/TNF hydrogel exhibited a significantly higher cell viability when compared with the CV-N solution. This supports the reported safety profile of tenofovir and the cytoprotective capability of the polymer systems as well as excipients used in the formulation of the hydrogel. Formulating drugs like Tenofovir and Cyanovirin-N within hydrogels can significantly reduce local concentration spikes and cytotoxic effects, thus enhances cell viability in in vitro models. Additionally, the hydrated matrix can stabilize sensitive proteins and create a more biocompatible microenvironment. While TNF/CV-N hydrogels may appear non-toxic in cell-based assays, the immune response due to inflammation was observed in rabbit vagina, a more complex model. Factors such as foreign-body recognition, immune cell activation, and degradation byproducts can contribute to inflammation, not usually observed *in vitro* models [55].

3.4.8. In-vivo safety assessment in rabbit model

The *in-vivo* cytotoxicity of the optimized hydrogel formulation (F1) in rabbit vagina was compared with that of 0.0005% CV-N (F2), 1% TNF (F3), Nonoxynol-9 (F4) and control group (F5) over 72 h (Fig. 8). The vagina tissue was sectioned into inner, middle and outer and photomicrographs (H & E × 100) of each section of the vaginal tissue were taken. The sectioned tissues were observed for epithelial exfoliation, vascular congestion, oedema, presence of inflammatory cells and the laminar propria. Fig. 8A–C shows the status of the stratified squamous epithelium, basal cell layer, and lamina propria 24 h after drug administration in comparism to that observed after 72 h post drug administration as seen in Fig. 8D–F.

After 24 h post treatment, groups administered with CV-N/TNF hydrogel (F1) showed greater exfoliation of the stratified squamous epithelium of the outer vagina and inflammation compared with the groups treated with 0.0005% CV-N only (F2) and 1% TNF only (F3). This is due to the combined toxic effect of the two moieties (TNF with CV-N). However, the toxicity observed in the control group treated with nonoxynol-9 (F4) was higher than in groups F1-F3. This suggests that hydrogel formulation is likely to cause only tolerable irritation when used vaginally in humans, as nonoxynol-9, despite causing slight vaginal toxicity has been commercially used with reports of high tolerance and user acceptance [56]. Moreover, the mild exfoliation of the outer squamous epithelium observed in the control group (F5) used to assess the impact of the administration device suggests that the toxicity observed for groups F1 to F4 are slightly less significant as the administration device may have contributed to irritation of the vaginal epithelium.

Following 72 h post administration of the drugs (Fig. 8D–F), toxicity observed at 24 h had significantly resolved in all treatment groups. This may be attributed to the clearance of the treatments administered at 72 h. The self-healing ability of the vagina tissue from mild to moderate irritation as well as localized immune response also plays a role as the inflammation observed at 24 h post treatment resolved. Moreover, damaged cells in the vagina were likely sloughed off and replaced by healthy cells [57].

3.5. Study limitations

The successful ANN guided optimization of the TNF/CV-N hydrogel formulation using the box Behnken model is not without its limitations.

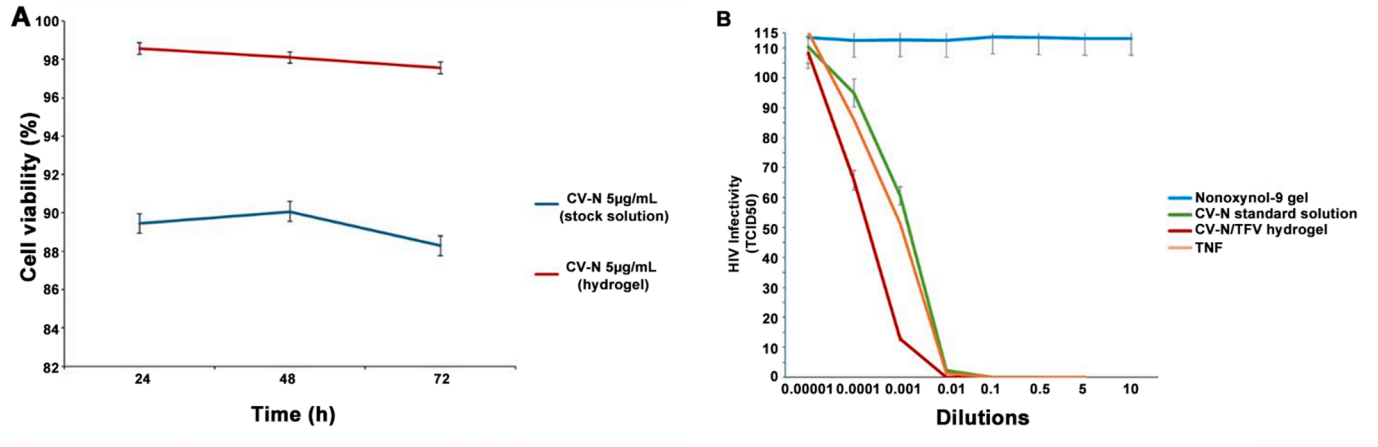

Fig. 7. (A) *In vitro* cell viability of optimized Hydrogel, CV-N using MTT cytotoxicity assay over 72 h *in vitro.* (B) HIV infectivity dose-response curves for optimized, CV-N/TNF Hydrogel, CV-N, TNF and nonoxynol gel incubated with HIV-1 indicator TZM-bl cells at different concentrations (n = 4).

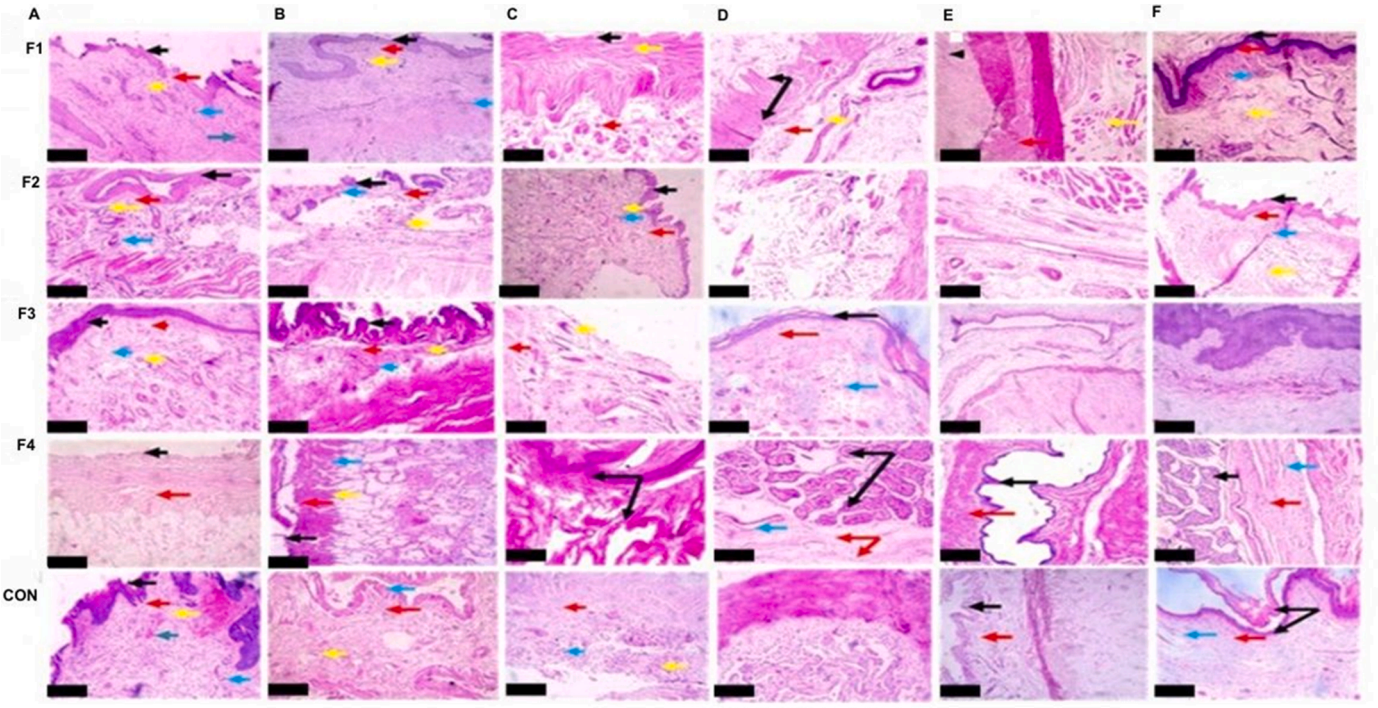

Fig. 8. Histological images stained with hematoxylin and eosin captured at an objective magnification of ×100. Showing the inner (A) middle (B), outer (C) vaginal tissue of rabbits after 24 h and inner (D), middle (E), outer (F) vaginal tissue of rabbits after 72 h of treatment with CV-N/TNF hydrogel (F1), 0.0005% CV-N, (F2), 1% TNF (F3), Nonoxynol-9 (F4) and Control. *Black arrow – epithelial exfoliation. Red arrow – lamina propria. Blue arrow – blood vessels. Yellow arrow – inflammatory cells. (Scale bar −100 µm).

The accuracy of model prediction is largely dependent on the experimental data quality and quantity used for algorithm training and validation; therefore, its predictive performance may decline when used beyond the tested range. Moreover, the Franz cell diffusion method utilized for drug release assay cannot perfectly replicate real life situations in the vagina as parameters such as enzymatic activity, vagina microbiome, pH changes might significantly affect the release of the incorporated TNF and CV-N. Also, the mucoadhesion and release assay method used did not take cognizance of the influence of semen and seminal fluid enzymes on these parameters and the incorporated CV-N and TNF which might be an important factor in real life situations. Future mucoadhesion and release assays should be designed to evaluate the influence of semen and seminal fluid enzymes, as these factors are critical in real-life scenarios and could significantly alter the release kinetics and stability of both TNF and CV-N. Incorporating these physiological variables will provide a more comprehensive understanding of the formulation's behavior post-application and guide the development of more effective and reliable multipurpose preventive technologies (MPTs).

4. Conclusion

Tenofovir and Cyanovirin-N loaded hydrogel was successfully formulated and optimized via analysis of the parameters such as high muco-adhesion of 96.1%, TNF flux 9806 µg/cm^2/h and TNF cumulative release 119, 205.6 µg/cm^2. These parameters serve as crucial factors enhancing the developed formulations efficacy in HIV and STI prophylaxis. The viscosity of the hydrogels ensures ease of administration and

immediate release of the incorporated moiety, while the high mucoadhesion ensures the hydrogel has prolonged contact time with the vaginal mucosa for efficacy. Histological studies of vaginal tissue post-treatment suggest the safety of the optimized hydrogel application. This formulation offers a powerful, on-demand STI prevention strategy, and marks a breakthrough in multipurpose prevention technologies.

Ethics approval and consent to participate

All animal tests were carried out in compliance with The National Institutes of Health guide for the care and use of laboratory animals and institutional guidelines approved in writing by Health Research Ethical Committee with approval number CMUL/HREC/012/23/1341.

CRediT authorship contribution statement

Karamot O. Oyediran: Writing – review & editing, Writing – original draft, Visualization, Validation, Resources, Project administration, Methodology, Investigation, Formal analysis, Data curation, Conceptualization. **Ibilola M. Cardoso-Daodu:** Writing – review & editing. **Peace Ofonabasi Bassey:** Writing – review & editing. **Deborah A. Ogundemuren:** Writing – review & editing, Conceptualization. **Ridwan Muhammed:** Writing – review & editing. **Olusola E. Ojo:** Visualization. **Andrew N. Amenaghawon:** Writing – original draft, Methodology, Data curation. **Chukwuemeka P. Azubuike:** Writing – review & editing, Supervision. **Rachna Agarwal:** Writing – review & editing, Conceptualization. **Kondoru Haritha:** Writing – review & editing. **Margaret O. Ilomunaya:** Writing – review & editing, Supervision, Resources, Methodology, Conceptualization.

Consent for publication

Not applicable.

Availability of data and material

The datasets used during the current study are available from the corresponding author on request.

Declaration of generative AI in scientific writing

The authors acknowledge the use of Image J, Canva, DPI converter to enhance images in this manuscript. ChatGPT was also used to summarize certain sentences. After using this tool/service, the author(s) reviewed and edited the content as needed and take(s) full responsibility for the content of the publication.

Cyanovirin-N was generously supplied by the BARC group, Mumbai, India. Financial support and access to Electospinnig equipment was provided by the MEDAFRICA GMP Laboaratory, Faculty of Pharmacy University of Lagos Nigeria.

Declaration of competing interest

The authors declare that they have no known competing financial interests or personal relationships that could have appeared to influence the work reported in this paper.

Acknowledgement

Cyanovirin-N was generously supplied by the BARC group, Mumbai, India. Financial support and access to the NLI Electrospinnig equipment was provided by the MEDAFRICA GMP Laboratory, Faculty of Pharmacy University of Lagos Nigeria. The authors acknowledge the support of the entire staff of Pharmaceutics and Pharmaceutical technology, Faculty of Pharmacy, University of Lagos

Appendix A. Supplementary data

Supplementary data to this article can be found online at https://doi.org/10.1016/j.pscia.2025.100079.

References

[1] D. Gökengin, T. Noori, A. Alemany, C. Bienkowski, G. Liegon, A.Ç. İnkaya, et al., Prevention strategies for sexually transmitted infections, HIV, and viral hepatitis in Europe, Lancet. Reg. Health - Eur. 34 (2023) 100738, https://doi.org/10.1016/j.lanepe.2023.100738.

[2] B.Y. Holt, J.A. Turpin, J. Romano, Multipurpose prevention technologies: opportunities and challenges to ensure advancement of the Most promising MPTs, Front. Reprod. Health 3 (2021) 704841, https://doi.org/10.3389/frph.2021.704841.

[3] E.E. Tolley, S. Li, S.Z. Zangeneh, M. Atujuna, P. Musara, J. Justman, S. Pathak, L.-G. Bekker, S. Swaminathan, J. Stanton, J. Farrior, N. Sista, Acceptability of a long-acting injectable HIV prevention product among US and African women: findings from a phase 2 clinical trial (HPTN 076), J. Int. AIDS Soc. 22 (10) (2019) e25408, https://doi.org/10.1002/jia2.25408.

[4] J.S. Hynes, J.M. Sales, A.N. Sheth, E. Lathrop, L.B. Haddad, Interest in multipurpose prevention technologies to prevent HIV/STIs and unintended pregnancy among young women in the United States, Contraception 97 (3) (2018) 277–284, https://doi.org/10.1016/j.contraception.2017.10.006.

[5] A. van der Straten, K. Agot, K. Ahmed, R. Weinrib, E.N. Browne, K. Manenzhe, F. Owino, J. Schwartz, A. Minnis, Team, on behalf of the T. S., The tablets, ring, injections as options (TRIO) study: what young African women chose and used for future HIV and pregnancy prevention, J. Int. AIDS Soc. 21 (3) (2018) e25094, https://doi.org/10.1002/jia2.25094.

[6] J. Ross, J. Stover, Use of modern contraception increases when more methods become available: analysis of evidence from 1982–2009, Glob. Health Sci. Pract. 1 (2) (2013) 203–212, https://doi.org/10.9745/GHSP-D-13-00010.

[7] I. Maier, G. Kontaxis, C. Zimmermann, C. Steininger, Cyanovirin-N binding to N-Acetyl-d-glucosamine requires carbohydrate-binding sites on two different protomers, Biochemistry 63 (10) (2024) 1270–1277, https://doi.org/10.1021/acs.biochem.4c00113.

[8] R. Agarwal, J. Trivedi, D. Mitra, High yield production of recombinant Cyanovirin-N (Antiviral lectin) exhibiting significant anti-HIV activity, from a rationally selected *Escherichia coli* strain, Process Biochem. 93 (2020) 1–11, https://doi.org/10.1016/j.procbio.2020.03.011.

[9] H. Lotfi, R. Sheervalilou, N. Zarghami, An update of the recombinant protein expression systems of Cyanovirin-N and challenges of preclinical development, Bioimpacts : BI 8 (2) (2017) 139, https://doi.org/10.15171/bi.2018.16.

[10] R.J. Shattock, J.P. Moore, Inhibiting sexual transmission of HIV-1 infection, Nat. Rev. Microbiol. 1 (1) (2003) 25–34, https://doi.org/10.1038/nrmicro729.

[11] S. Xiong, J. Fan, K. Kitazato, The antiviral protein cyanovirin-N: the current state of its production and applications, Appl. Microbiol. Biotechnol. 86 (3) (2010) 805–812, https://doi.org/10.1007/s00253-010-2470-1.

[12] C.C. Tsai, P. Emau, Y. Jiang, B. Tian, W.R. Morton, K.R. Gustafson, et al., Cyanovirin-N gel as a topical microbicide prevents rectal transmission of SHIV89.6P in macaques, AIDS Res. Hum. Retrovir. 19 (7) (2003) 535–541, https://doi.org/10.1089/088922203322230897.

[13] M. Mazalovska, J.C. Kouokam, Lectins as promising therapeutics for the prevention and treatment of HIV and other potential coinfections, BioMed Res. Int. (2018) 3750646, https://doi.org/10.1155/2018/3750646.

[14] S.S.A. Abdool Karim, Q.A. Karim, A.B.M. Kharsany, C. Baxter, A.C. Grobler, L. Werner, et al., Tenofovir gel for the prevention of Herpes simplex virus type 2 infection, N. Engl. J. Med. 373 (6) (2015) 530–539, https://doi.org/10.1056/NEJMoa1410649.

[15] J. Wang, S.A. Khan, S. Yasmin, M.M. Alam, H. Liu, U. Farooq, et al., Central composite design [CCD]-response surface methodology [RSM] for modeling and simulation of MWCNT-Water nanofluid inside hexagonal cavity: application to electronic cooling, Case Stud. Therm. Eng. 50 (2023) 103488, https://doi.org/10.1016/j.csite.2023.103488.

[16] M. Kumar Ananthu, P. Kumar Chintamaneni, S. Basha Shaik, R. Thadipatri, N. Mahammed, Artificial neural networks in optimization of pharmaceutical formulations, Saudi. J. Med. Pharm. Sci. 7 (8) (2021) 368–378, doi:SJMPS_78_368-378c.pdf.

[17] H.S. Kusuma, A.N. Amenaghawon, H. Darmokoesoemo, Y.A.B. Neolaka, B. A. Widyaningrum, S.U. Onowise, et al., A comparative evaluation of statistical empirical and neural intelligence modeling of manihot esculenta-derived leaves extract for optimized bio-coagulation-flocculation of turbid water, Ind. Crop. Prod. 186 (2022) 115194, https://doi.org/10.1016/j.indcrop.2022.115194.

[18] S. Sukpancharoen, T. Katongtung, N. Rattanachoung, N. Tippayawong, Unlocking the potential of transesterification catalysts for biodiesel production through machine learning approach, Bioresour. Technol. 378 (2023) 128961, https://doi.org/10.1016/j.biortech.2023.128961.

[19] A.N. Amenaghawon, S. Igemhokhai, S.A. Eshiemogie, F. Ugbodu, N. I. Evbarunegbe, Data-driven intelligent modeling, optimization, and global sensitivity analysis of a xanthan gum biosynthesis process, Heliyon 10 (3) (2024) e25432, https://doi.org/10.1016/j.heliyon.2024.e25432.

[20] M. Ekpenyong, A. Asitok, U. Ben, A. Amenaghawon, H. Kusuma, A. Akpan, et al., Application of the novel manta-ray foraging algorithm to optimize acidic peptidase production in solid-state fermentation using binary agro-industrial waste, Prep.

Biochem. Biotechnol. 54 (2) (2024) 226–238, https://doi.org/10.1080/10826068.2023.2214936.
[21] M. Ilomuanya, A. Amenaghawon, J. Odimegwu, O. Okubanjo, C. Aghaizu, A. Oluwatobiloba, et al., Formulation and optimization of gentamicin hydrogel infused with tetracarpidium conophorum extract via a central composite design for topical delivery, Turk. J. Pharm. Sci. 15 (3) (2018) 319–327, https://doi.org/10.4274/tjps.33042.
[22] W. Alshaer, H. Nsairat, Z. Lafi, O.M. Hourani, A. Al-Kadash, E. Esawi, et al., Quality by design approach in liposomal formulations: robust product development, Molecules 28 (1) (2023) 10, https://doi.org/10.3390/molecules28010010.
[23] M.O. Ilomuanya, P.O. Bassey, D.A. Ogundemuren, U.N. Ubani-Ukoma, A. Tsamis, Y. Fan, et al., Development of mucoadhesive electrospun scaffolds for intravaginal delivery of lactobacilli spp., a tenside, and metronidazole for the management of bacterial vaginosis, Pharmaceutics 15 (4) (2023) 1263, https://doi.org/10.3390/pharmaceutics15041263.
[24] M.O. Ilomuanya, R. Elesho, A. Amenaghawon, A. Adetuyi, V. Velusamy, S. Akanmu, Development of trigger sensitive hyaluronic acid/palm oil-based organogel for in vitro release of HIV/AIDS microbicides using artificial neural networks, Future J. Pharm. Sci. 6 (2020) 1, https://doi.org/10.1186/s43094-019-0015-8.
[25] R. Gawali, J. Trivedi, S. Bhansali, R. Bhosale, D. Sarkar, D. Mitra, Design, synthesis, sdocking studies and biological screening of 2-thiazolyl substituted -2,3-dihydro-1H-naphtho[1,2-e][1,3]oxazines as potent HIV-1 reverse transcriptase inhibitors, Eur. J. Med. Chem. 157 (2018) 310–319, https://doi.org/10.1016/j.ejmech.2018.07.067.
[26] M.O. Ilomuanya, B.B. Salako, M.O. Ologunagba, O.O. Shonekan, K. Owodeha-Ashaka, E.S. Osahon, et al., Formulation and optimization of metronidazole and lactobacillus spp. layered suppositories via a three-variable, five-level central composite design for the management of bacterial vaginosis, Pharmaceutics 14 (11) (2022) 2337, https://doi.org/10.3390/pharmaceutics14112337.
[27] N.F. Che Nan, N. Zainuddin, Ayob M. Ahmad, Preparation and swelling study of CMC hydrogel as potential superabsorbent, Pertanika J. Sci. Technol. 27 (1) (2019) 489–498. http://psasir.upm.edu.my/id/eprint/67245.
[28] S. Gedam, P. Jadhav, S. Talele, A. Jadhav, Effect of crosslinking agent on development of gastro-retentive mucoadhesive microspheres of risedronate sodium, Int. J. Appl. Pharm. 10 (2018) 133, https://doi.org/10.22159/ijap.2018v10i4.26071.
[29] N.F.A.Z. Tuan Mohamood, A.H. Abdul Halim, N. Zainuddin, Carboxymethyl cellulose hydrogel from biomass waste of oil palm empty fruit bunch using calcium chloride as crosslinking agent, Polymers 13 (23) (2021) 4056, https://doi.org/10.3390/polym13234056.
[30] N.A. Peppas, Y. Huang, Nanoscale technology of mucoadhesive interactions, Adv. Drug Deliv. Rev. 56 (11) (2004) 1675–1687, https://doi.org/10.1016/j.addr.2004.03.001.
[31] B.J. Moncla, K. Pryke, L.C. Rohan, H. Yang, Testing of viscous anti-HIV microbicides using lactobacillus, J. Microbiol. Methods 88 (2) (2012) 292–296, https://doi.org/10.1016/j.mimet.2011.12.013.
[32] H. Park, J.R. Robinson, Mechanisms of mucoadhesion of poly [acrylic acid] hydrogels, Pharm. Res. 4 (6) (1987) 457–464, https://doi.org/10.1023/a:1016467219657.
[33] V.K. Yadav, A.B. Gupta, R. Kumar, J.S. Yadav, B. Kumar, Mucoadhesive polymers: means of improving the mucoadhesive properties of drug delivery system, J. Chem. Pharmaceut. Res. 2 (5) (2010). https://www.researchgate.net/publication/222712279_Mucoadhesive_Polymers_Means_of_Improving_the_Mucoadhesive_Properties_of_Drug_Delivery_System.
[34] M. Momoh, M. Adikwu, C. Ibezim, K. Ofokansi, A. Attama, Thermal characterisation of PEGylated mucin, Asian Pac. J. Tropical Med. 3 (6) (2010) 458–460, https://doi.org/10.1016/S1995-7645(10)60110-1.
[35] T. Crouzier, K. Boettcher, A.R. Geonnotti, N.L. Kavanaugh, J.B. Hirsch, K. Ribbeck, et al., Modulating mucin hydration and lubrication by deglycosylation and polyethylene glycol binding, Adv. Mater. Interfac. 2 (18) (2015) 1500308, https://doi.org/10.1002/admi.201500308.
[36] X. Li, J.P. Gong, Design principles for strong and tough hydrogels, Nat. Rev. Mater. (2024) 1–19, https://doi.org/10.1038/s41578-024-00672-3.
[37] E.M. Ahmed, Hydrogel: Preparation, characterization, and applications: a review, J. Adv. Res. 6 (2) (2015) 105, https://doi.org/10.1016/j.jare.2013.07.006.
[38] D. Palmer, M. Levina, A. Nokhodchi, D. Douroumis, T. Farrell, A. Rajabi-Siahboomi, The influence of sodium carboxymethylcellulose on drug release from polyethylene oxide extended-release matrices, AAPS PharmSciTech 12 (3) (2011) 862, https://doi.org/10.1208/s12249-011-9648-4.
[39] R. Reeves, A. Ribeiro, L. Lombardo, R. Boyer, J.B. Leach, Synthesis and characterization of carboxymethylcellulose-methacrylate hydrogel cell scaffolds, Polymers 2 (3) (2010) 252–264, https://doi.org/10.3390/polym2030252.
[40] X. Li, C. Cao, D. Yuan, Q. Liu, J. Zhao, Effects of the incorporation of calcium chloride on the physical and oxidative stability of filled hydrogel particles, Foods 11 (3) (2022) 278, https://doi.org/10.3390/foods11030278.
[41] G. Cheraghian, M.P. Wistuba, S. Kiani, A.R. Barron, A. Behnood, Rheological, physicochemical, and microstructural properties of asphalt binder modified by fumed silica nanoparticles, Sci. Rep. 11 (1) (2021) 11455, https://doi.org/10.1038/s41598-021-90620-w.
[42] A.R. Cho, Y.G. Chun, B.K. Kim, D.J. Park, Preparation of alginate–CaCl2 microspheres as resveratrol carriers, J. Mater. Sci. 49 (13) (2014) 4612–4619, https://doi.org/10.1007/s10853-014-8163-x.
[43] M. Vigata, C. Meinert, D.W. Hutmacher, N. Bock, Hydrogels as drug delivery systems: a review of current characterization and evaluation techniques, Pharmaceutics 12 (12) (2020) 1188, https://doi.org/10.3390/pharmaceutics12121188.
[44] Y. Fu, W.J. Kao, Drug release kinetics and transport mechanisms of non-degradable and degradable polymeric delivery systems, Expet Opin. Drug Deliv. 7 (4) (2010) 429–444, https://doi.org/10.1517/17425241003602259.
[45] S. Ayehunie, Y.Y. Wang, T. Landry, S. Bogojevic, R.A. Cone, Hyperosmolal vaginal lubricants markedly reduce epithelial barrier properties in a three-dimensional vaginal epithelium model, Toxicol. Rep. 5 (2017 Dec 16) 134–140, https://doi.org/10.1016/j.toxrep.2017.12.011.
[46] S. Singh, A.K. Dash, Physical Properties, their Determination, and Importance in Pharmaceutics. Pharmaceutics: Basic Principles and Application to Pharmacy Practice, second ed., 2023, pp. 67–113.
[47] S.A. Khan, S.B. Khan, L.U. Khan, A. Farooq, K. Akhtar, A.M. Asiri, Fourier transform infrared spectroscopy: fundamentals and application in functional groups and nanomaterials characterization, in: S.K. Sharma (Ed.), Handbook of Materials Characterization, Springer International Publishing, Cham, 2018, pp. 317–344, https://doi.org/10.1007/978-3-319-92955-2_9.
[48] B. Kumar, R. Priyadarshi, S. Singh, F. Deeba, A. Kulshreshtha, K. Gaikwad, et al., Nanoporous sodium carboxymethyl Cellulose-g-poly [sodium Acrylate]/FeCl3 hydrogel beads: synthesis and characterization, Gels 6 (2020) 49, https://doi.org/10.3390/gels6040049.
[49] P. Rantuch, The thermal degradation of polymer materials, in: P. Rantuch (Ed.), Ignition of Polymers, Springer International Publishing, Cham, 2022, pp. 1–43, https://doi.org/10.1007/978-3-031-13082-3_1.
[50] M.A. Saad, E.R. Sadik, B.M. Eldakiky, H. Moustafa, E. Fadl, Z. He, et al., Synthesis and characterization of an innovative sodium alginate/polyvinyl alcohol bioartificial hydrogel for forward-osmosis desalination, Sci. Rep. 14 (1) (2024) 8225, https://doi.org/10.1038/s41598-024-58533-6.
[51] A. Hotter, H. Lengauer, Crystalline forms of tenofovir alafenamide monofumarate, WO2017134089A1, https://patents.google.com/patent/WO2017134089A1/en, 2017.
[52] C.A. Bewley, K.R. Gustafson, M.R. Boyd, D.G. Covell, A. Bax, G.M. Clore, et al., Solution structure of Cyanovirin-N, a potent HIV-Inactivating protein, Nat. Struct. Biol. 5 (7) (1998) 571–578. https://www.nature.com/articles/nsb0798_571.
[53] E.G. Raymond, C.P. Lien, J. Luoto, Contraceptive effectiveness and safety of five nonoxynol-9 spermicides: a randomized trial, Obstet. Gynecol. 103 (3) (2004) 430–439, https://doi.org/10.1097/01.AOG.0000113620.18395.0b.
[54] P. Kumar, A. Nagarajan, P.D. Uchil, Analysis of cell viability by the MTT assay, Cold Spring Harb. Protoc. 6 (2018), https://doi.org/10.1101/pdb.prot095505.
[55] A.J. Dominijanni, M. Devarasetty, S.D. Forsythe, K.I. Votanopoulos, S. Soker, Cell viability assays in three-dimensional hydrogels: a comparative study of accuracy, Tissue Eng. C Methods 27 (7) (2021) 401, https://doi.org/10.1089/ten.tec.2021.0060.
[56] E.M. Wilkinson, P. Łaniewski, M.M. Herbst-Kralovetz, R.M. Brotman, Personal and clinical vaginal lubricants: impact on local vaginal microenvironment and implications for epithelial cell host response and barrier function, J. Infect. Dis. (12) (2019) 220, https://doi.org/10.1093/infdis/jiz412.
[57] E. Amabebe, D.O.C. Anumba, The vaginal microenvironment: the physiologic role of lactobacilli, Front. Med. 5 (2018) 181, https://doi.org/10.3389/fmed.2018.00181.